Volume 54 · April 2013

ISSN 0008-6223

an international journal

Carbon

Reporting research on Carbonaceous Materials,
their Production, Properties and Applications

Cut CNTs

100 nm

Editors-in-Chief: R.H. Hurt and P.A. Thrower

Available online at www.sciencedirect.com

SciVerse ScienceDirect

Theoretical study of strained porous graphene structures and their gas separation properties

Sirichok Jungthawan [a,b,*], Pakpoom Reunchan [c], Sukit Limpijumnong [a,b]

[a] School of Physics, Institute of Science, Suranaree University of Technology, Nakhon Ratchasima 30000, Thailand
[b] Thailand Center of Excellence in Physics (ThEP), Commission on Higher Education, Bangkok 10400, Thailand
[c] Department of Physics, Faculty of Science, Kasetsart University, Bangkok 10900, Thailand

ARTICLE INFO

ABSTRACT

The structural deformation of porous graphene (PG) under tensile stress and the diffusion properties of H_2, O_2 and CO_2 through PG under different strain conditions have been investigated using the first-principles density functional theory. It is found that the application of a tensile stress can effectively increase the diffusion rate of H_2, O_2, and CO_2 in PG by up to 7, 13, and 20 orders of magnitude, respectively. Therefore, we propose that applying tensile stress is an effective way to control the diffusion rate of gases through PG. By applying sufficiently large tensile stress, one might able to use PG for filtering larger gas molecules such as O_2 in addition to previously proposed H_2. The results open up an opportunity to utilize PG as a controllable gas separation membrane, leading to wide range of energy and environmental applications.

© 2012 Elsevier Ltd. All rights reserved.

1. Introduction

The fabrication of nanostructure by the bottom-up approaches paves a way to actually utilize nanomaterials [1–6]. Ultraviolet-induced oxidative etching [7,8] and lithographic techniques [9,10] that are generally referred to as top–down approaches, can be effectively used to produce fine structures down to a microscopic scale. However, at the nanoscale, such techniques faced serious precision and resolution limitations. On the other hand, the concept of materials engineering with molecular building-block has been proposed to be a promising way to fabricate nanoscale systems [1,2,5,6]. Recently, the porous form of graphene [11–13] with a regular pore-size distribution has been synthesized by a bottom-up approach using the chemical building blocks of functionalized phenyl rings [3,14]. A 2-dimensional (2D) network of a covalently-linked hydrocarbon superstructure was grown spontaneously on a silver substrate based on molecular self-assembly. The molecules resemble to form graphene-like flakes with regular pores distributed; called porous graphene (PG) [3]. The typical size of PG is around 50 nm^2. The unit cell of PG is equivalent to a 3×3 supercell of the graphene unit cell with one hexagon pore created and decorated by six hydrogen atoms as shown in Fig. 1a. Because of these well-defined pore size and distribution, PG is a prime candidate to be utilized as a gas-separation membrane, [15,16] due to its exceptionally highly selectivity of H_2 among other atmospheric gases. PG has been proposed to be a viable membrane for gas separation due to its high permeability of H_2 [7] and almost completely block other gases with the selectivity on the order of 10^{26} for H_2/CO_2 [15]. This makes PG a high potential candidate material for technological applications such as hydrogen storage [15,17,18], fuel cells [15,16], and gas sensors [15,16].

The pore size and the functionalization of the pore introduced to graphene strongly affect the diffusion properties and the characteristics of the membrane [15,16,19,20]. In principle, membranes with different pore characteristics could be designed from chemical building block or electron beam
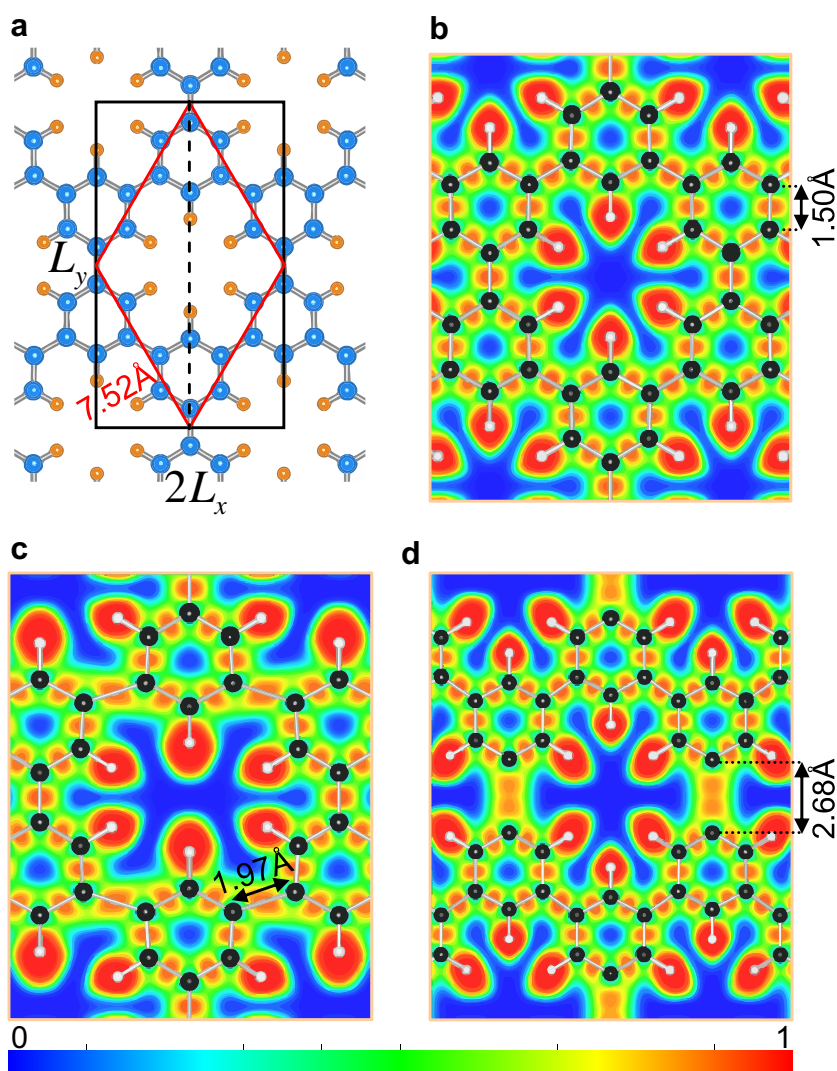
Fig. 1 – (a) The unit cell of porous graphene (indicated by a red rhombus). The electron localization function (see text) are plotted for (b) unstrained porous graphene, (c) 20% strain in zigzag (x) direction ($\varepsilon_x = 0.20$), and (d) 20% strain in armchair (y) direction ($\varepsilon_y = 0.20$). (For interpretation of the references to color in this figure legend, the reader is referred to the web version of this article.)

irradiation [9] to suite different requirements of each application. However, in practice, it could be highly challenging to engineer the pores of graphene. Here, we propose an alternative way to control the characteristics and the gas diffusion properties of the PG without the need to modify the structure or functionalization of PG pores. We will show, based on first principles calculations, that the characteristics and the gas diffusion properties of the PG can be tuned by applying reasonable strain to the membrane. While we focus our attentions on the effects of strain on diffusion properties of CO_2, O_2, and H_2 gases, the application of such idea can be applied to other gases as well.

2.   Computational methods

The calculations were performed based on the density functional theory [21] as implemented in the VASP code [22–24], within the Perdew, Burke, and Erzenhoff (PBE) [25] functional form of the generalized gradient approximation (GGA) [26] and the projector augmented wave (PAW) potentials [27,28]. The cutoff energy of the plane wave expansion is 600 eV. Structural relaxation is performed until the force on each ion is below 0.01 eV/Å. The unit cell of PG is constructed from a 3×3 repetition of the primitive unit cell of graphene with six carbon atoms removed to create a pore and the pore edges are decorated by six hydrogen atoms as shown in Fig. 1a. The vacuum spacing of 20 Å is used to prevent fictitious interactions between the adjacent layers in the calculations. The Γ-centered Monkhorst–Pack k-mesh of $6 \times 6 \times 1$ is used for Brillouin zone integrations.

3.   Results and discussion

The optimized lattice parameter for unstrained PG is 7.517 Å which is in good agreement with known experimental value (7.4 Å [3]) and other calculated values (7.45 Å [29] and

7.455 Å [15]). Based on the symmetries, there are two non-equivalent C–C bonds with the calculated bond distances of 1.404 Å and 1.497 Å (the longer one is the one connecting two hexagons). The calculated C–H bond length is 1.086 Å. The elastic properties of PG were studied by applying the uniaxial strain along the two most relevant directions, i.e. zigzag (x) and armchair (y). The uniaxial strain is defined as the ratio of deformation ΔL to the initial length L, i.e., $\varepsilon_i = \Delta L_i / L_i$ where $i = x, y$. The optimized unstrained cell parameters of PG were $L_x = 3.758$ Å and $L_y = 13.019$ Å, as shown in Fig. 1a. The number of pore per unit area (pore density) is then simply $(L_x L_y)^{-1}$. The limit of structural deformation of PG under applied strain can be evaluated by inspecting the electron localization function (ELF) [30,31]. ELF has values between 0 and 1, where 1 corresponds to perfect localization and 1/2 corresponds to electron–gas-like pair probability [30,31]. Fig. 1b shows the ELF of unstrained PG. The high electron localization at the center of C–C bonds indicates the character of covalent bonds where the electrons are shared between two carbons which reflects the carbon bonding. Under tensile strains some of the C–C bonds, depending on tensile directions, are extended and the ELF shapes at those bonds are distorted. These effects are especially obvious at large strain. Fig. 1c illustrates the ELF of PG under 20% tensile strain along the zigzag direction ($\varepsilon_x = 0.20$). The C–C bonds connecting two hexagons are significantly elongated by about 32% to 1.970 Å. The ELF at the center of those bonds are clearly broadened but does not split; indicating that the covalent bonds still existed. On the other hand, for PG under 20% tensile strain along the armchair direction ($\varepsilon_y = 0.20$), the C–C bonds are elongated even more, i.e., by 79% to 2.680 Å. The ELF at the center of the bonds splits into two equal parts having a minimum between the two carbons as shown in Fig. 1d; indicating the break-down of the C–C covalent bonds. Note, however, that under strains the other C–C bonds are nearly intact. These simple investigations suggest that PG can withstand higher tensile loading along the zigzag direction than the armchair direction.

We have studied the PG under strain in both directions in details by varying the uniaxial strain in the range of −20% to 20%, i.e., $\varepsilon_i = \pm 0.2$. The total energies of strained configurations ($\varepsilon_x, \varepsilon_y$) in the range above were calculated using uniform meshes with $\Delta\varepsilon = 0.1$. To gain detailed data near the unstrained region, a finer mesh with $\Delta\varepsilon = 0.02$ were used for low strain regions ($\varepsilon_i = \pm 0.1$). The discrete set of the strained-PG calculations is interpolated to a smooth surface [32]. Fig. 2a shows the energy of a strained PG as a function of strain $E(\varepsilon)$ referenced to the unstrained one $E(\varepsilon = 0)$.

From the full energy surface as a function of strain, the information of lateral relaxation when the uniaxial strain is applied can be extracted. For each applied strain, the lateral side will relax to lower the energy. Therefore, the optimized lateral strain is defined at the lowest energy for a given applied strain. Under uniaxial strain ε_x (or ε_y) the optimized energy is shown as a curve in Fig. 2a. The two curves can be written as,

$$\varepsilon_y(\varepsilon_x) = -0.279\varepsilon_x + 0.493\varepsilon_x^2 + 0.504\varepsilon_x^3 \qquad (1)$$

$$\varepsilon_x(\varepsilon_y) = -0.275\varepsilon_y + 0.902\varepsilon_y^2 + 0.153\varepsilon_y^3 \qquad (2)$$

When the PG is stretched in one direction, the lateral side would shrink. Such relation is reflected in the Poisson's ratio [33]. To gain insights on structural deformation, we defined *the ratio of the change in the applied strain* in the x and y directions as $v_x = -d\varepsilon_y/d\varepsilon_x$ (along the path defined by Eq. (1)) and $v_y = -d\varepsilon_x/d\varepsilon_y$ (along the path defined by Eq. (2)), respectively. The ratio of zero would mean that applying a strain in one direction does not affect the lateral direction at all. From the plot in Fig. 2b, we can see that the ratio is positive and decreases with increasing (stretch) strain. This means that initially the lateral side would relax in order to reduce area expansion. However, as the PG is stretched more, the PG started to lose its stiffness and the ratio changes sign. We can also see that v_y turns lower than v_x at large tensile strain and crosses zero at $\varepsilon_y = 0.14$.

The plot of strain energy (E_S) as a function of applied uniaxial strain (ε) as well as its first-derivative ($E_S' = dE_S/d\varepsilon$) along the paths given by Eqs. (1) and (2) are shown in Fig. 2c. E_S in both directions are similar at low strain, i.e., $\varepsilon_i < 0.08$, and started to be different at higher strain. The ultimate strength of PG can be estimated from the critical value of E_S'. From Fig. 2c, the ultimate strength of PG under tensile strain along the armchair direction corresponds to $\varepsilon_y = 0.14$ which agrees with the point where the v_y turns zero. For the zigzag direction, the ultimate strength corresponds to $\varepsilon_x = 0.19$. These results indicate that PG can withstand the strain up to about 14% in the y direction and 19% in the x direction. The forces associated with the strain can be calculated from $f_x = \frac{\ell_y}{L_y} \frac{dE_S}{L_x d\varepsilon_x}$ and $f_y = \frac{\ell_x}{L_x} \frac{dE_S}{L_y d\varepsilon_y}$ where ℓ_x and ℓ_y are the dimension of the PG membrane along zigzag and armchair direction, respectively. For example, for a PG membrane with the length of 5 nm along the armchair direction ($\ell_y = 5$ nm) the force of about 50 nN is required to cause stretch strain of 10% along the zigzag (x) direction.

For a small strain ($\varepsilon_i < 0.04$), the first derivative of energy-strain curve is linear (with a slope of about 350 eV/unit cell), as show in Fig. 2c. However, at a larger strain ($\varepsilon_i > 0.04$) the slope decreases; indicating that it becomes easier to deform. According to Şahin et al. [34], the energy-strain relationship can be fitted with the equation $E_S = a_1\varepsilon_x^2 + a_2\varepsilon_y^2 + a_3\varepsilon_x\varepsilon_y$. For $\varepsilon_i < 0.04$, a_1 can be approximated to be equal to a_2 due to the isotropy of the structure. The in-plane stiffness can be calculated by $C = (1/A_0)(\partial^2 E_S/\partial\varepsilon^2) = [2a_1 - (a_3)^2/2a_1]/A_0$ where $A_0 = L_x L_y$ is the area of unstrained system. In our case, the fitted values (per unit cell) are $a_1 = a_2 = 196.56$ eV, $a_3 = 108.29$ eV, and $A_0 = 48.925$ Å^2, respectively. We obtained the in-plane stiffness of the PG of 120 N/m. In comparison with graphene, the pores make the PG 64% weaker than graphene (335 N/m [34], 340 ± 40 N/m [35]). Other compounds with 2D honeycomb structure are BN, graphane, SiC, and Si. Their calculated elastic stiffness values are 267, 243, 166, and 62 N/m, respectively [36]. We can see that PG is still tough with the elastic stiffness comparable to SiC and higher than Si.

Next, we investigate PG membrane for gas separation purpose by studying the diffusion barrier of several gas molecules in the range of uniaxial strain from −4% to +10%. A supercell (2×2 of the unit cell of PG) is used for the calculation of the diffusion barrier of H_2, O_2, and CO_2 molecule passing through PG. Previous studies showed that these small molecules will pass through the PG with its axis perpendicular to the sheet
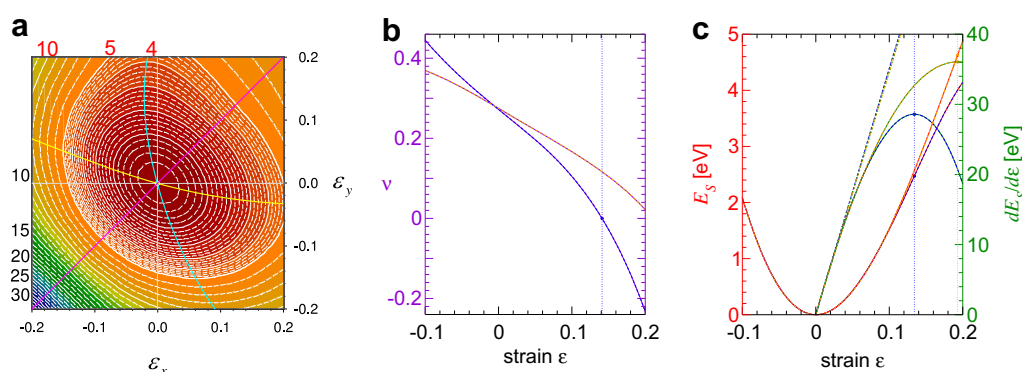
Fig. 2 – (a) The strain energy surface in eV/unit cell. The optimized paths with uniaxial strain in x (yellow) and y (blue) axis and symmetrical strain (pink) are shown. The solid contour line is 1 eV and 5 eV increment for $E_S < 5$ and $E_S > 5$, respectively. (b) The ν value (see text) under uniaxial strain in x (dashed orange-violet curve) and y (dashed blue-violet curve), dotted line indicates the point where $\nu_y = 0$ ($\varepsilon_y = 0.14$). (c) The strain energy E_S (left axis) and its derivative (right axis) along the optimized uniaxial strain path in x (dashed orange curve) and y (dashed blue curve). The dotted lines indicate critical strains at $\varepsilon_x = 0.19$ (orange) and $\varepsilon_y = 0.13$ (blue). (For interpretation of the references to color in this figure legend, the reader is referred to the web version of this article.)
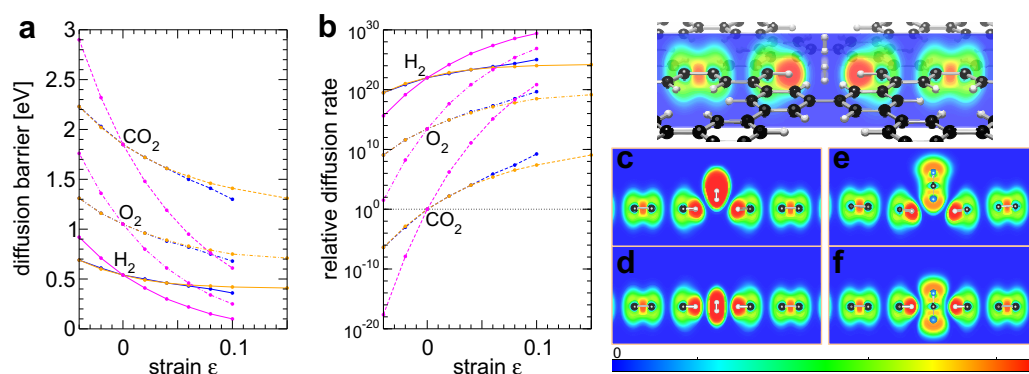

Fig. 3 – (a) Diffusion barrier of H_2 (solid line), O_2 (dot-dashed line), and CO_2 (dashed line) with uniaxial strain in x (orange) and y (blue) directions, and symmetrical strain (pink). (b) Relative diffusion rate referenced to the diffusion rate of CO_2 in unstrained PG. (c–f) The electron localization function showing the diffusion of H_2 and CO_2 through an unstrained PG. (c and e) show H_2 and CO_2 at 0.8 Å away from the PG. (d and f) show H_2 and CO_2 at the center of the pore. (For interpretation of the references to color in this figure legend, the reader is referred to the web version of this article.)

[15,16,19] as illustrated for H_2 in the inset of Fig. 3. For the studied molecules, it was found that the molecular diffusion pathway has the lowest diffusion barrier when the transition state is at the center of the pore. Therefore, the diffusion barrier is defined as the difference in total energy when the molecule is at the center of the pore and when the molecule is at the energetically favorable distance from the pore. For the unstrained PG ($\varepsilon = 0$), our calculated diffusion barrier of H_2, O_2, and CO_2 molecules are 0.54, 1.05, and 1.85 eV, respectively, which are comparable to the values obtained in the previous works [15,16]. Based on these big differences in the diffusion barriers, Li et al. proposed that PG can be used for gas filtering with the relative diffusion rate as large as 10^{26} for the diffusion of H_2 relative to CO_2 [15]. Changing functionalize element, for e.g., decorating the pore with N instead of H, is one of the proposed approaches to modify the gas diffusion properties of graphene membrane [19]. Here, we studied the effects of strain on the diffusion properties. This would allow direct control or fine tune of the diffusion properties of the PG membrane.

Fig. 3a shows the diffusion barriers of PG as a function of three types of strain for H_2, O_2 and CO_2 molecules. At low uniaxial strain ($\varepsilon < 0.08$), the diffusion barriers as a function of strain in both directions are nearly identical. The difference only takes place at a larger strain where the pore shapes are significantly deformed in a different way. At large strain, the PG with tensile strain in the y direction has lower diffusion barriers than that with strain applied in the x direction. This is due to the larger pore expansion due to the larger C–C bond extension as shown in Fig. 1d. For the PG with strain in the x direction, the reduction in the barrier saturated at a value of 0.41, 0.71, and 1.31 eV for H_2, O_2, and CO_2, respectively at $\varepsilon_x = 0.10$. This is because the tensile strain expands the pores in one direction while the transverse direction of the pores is initially shrunk by a small amount forming a slit-shape pore which is nearly unchanged at large strain. This can be seen

from the v value in Fig. 2b, and the characteristic curve in Fig. 2a where the deformation in the lateral direction is slightly changes and saturated at larger strain. Under the symmetrical strain, where the PG is stretched symmetrically in both directions, the diffusion barrier reduced much faster than the uniaxial strain because the pore is symmetrically expanded. The diffusion barrier of H_2, O_2, and CO_2 at $\varepsilon = 0.10$ are reduced to 0.10, 0.25, and 0.61 eV, respectively. It is interesting to note that the diffusion barriers of O_2 and CO_2 reduce as a function of strain faster than that of the H_2 molecule. This opens up an opportunity not only to tune the diffusion rate but also to tune the gas selectivity of PG by strains.

The diffusion rate of a gas passing through PG is a function of the diffusion barrier. Here, we defined the selectivity (relative diffusion rate) of PG for the diffusion of molecule X ($X = H_2$, O_2 and CO_2) under applied strain relative to the CO_2 diffusion rate of unstrained PG as,

$$S_X = \frac{r_X(\varepsilon)}{r_{CO_2}(\varepsilon = 0)} = \frac{A_X \exp[-E_X(\varepsilon)/k_B T]}{A_{CO_2} \exp[-E_{CO_2}(\varepsilon = 0)/k_B T]}, \quad (3)$$

where $E_X(\varepsilon)$ is the diffusion barrier of molecule X under applied strain ε, k_B is the Boltzmann constant, T is the temperature, and A_X is the diffusion prefactor. For simplicity we assumed the same values of the prefactor for the three gases and assumed that they are independent of strain ($A_X/A_{CO_2} = 1$) [15], and the temperature T is 300 K. The relative diffusion rates (Eq. (3)) as a function of the applied strain are plotted in Fig. 3b. For unstrained PG, the selectivity of H_2/CO_2 and O_2/CO_2 is 10^{22} and 10^{13}, indicating an extremely high selectivity of H_2. The selectivity is significantly improved with compressive strain. Note, however that, in practice, the application of compressive strain to a thin layer PG is almost impossible. With the tensile strain, the diffusion rate can be significantly improved, i.e., up to 2, 5, and 9 orders of magnitude for H_2, O_2, and CO_2, respectively (calculated at $\varepsilon_x = 0.15$). This can significantly improve the diffusion yield although the selectivity will be slightly affected. This is because the diffusion rates of the larger molecules (CO_2 and O_2) are significantly increases compared to that of the smaller molecules (H_2). As a result, the selectivity for H_2/CO_2 and O_2/CO_2 decreases to 10^{15} and to 10^{10}, respectively. However, such values of selectivity are still more than sufficient for most filtering applications. Moreover, by controlling the strain, one can increase the diffusion rate of O_2 by up to almost a million fold; opening up the opportunity to use PG to filter O_2 out from CO_2 and other larger gases.

For PG under symmetrical strain, the diffusion rates of H_2, O_2, and CO_2 can increase up to 7, 13, and 20 orders of magnitude, respectively (calculated at $\varepsilon = 0.10$). As can be seen in Fig. 3b, with increasing strain, the diffusion rate of O_2 and CO_2 increases faster than the rate of H_2. This is similar to the uniaxial strain cases. To understand why the strain affected the diffusion barrier of CO_2 more than H_2, we investigated the ELFs of the system before and during the diffusion as shown in Fig. 3c–f. We can see that the electron distributions of H_2 are localized around the molecule. As the molecule passes through the pore, it causes only little distortion on the electron distributions of the H atoms around the pore, indicating that the pore of unstrained PG is sufficiently large to

accommodate the diffusion of H_2 molecule. As a result, the barrier is barely reduced with the increasing pore size. On the other hand, for CO_2, the molecule largely affects the electron distributions around the pore and even pushes the dangling H atoms away from their original locations. As the pore size increased or distorted some or all of the surrounding H atoms are moved further away from the pore center. This reduces the interaction between the CO_2 and the surrounding H atoms, resulting in the significant reduce of the diffusion barrier.

Our calculations showed that the strain on PG can be used effectively to modify its diffusion barriers for H_2, O_2, and CO_2 such that the diffusion rates can be modified by several orders of magnitude. This opens up an opportunity to manipulate PG for the filtration applications of gases that are larger than H_2, such as O_2 from other larger molecules. While our calculations are limited to only three gas molecules, the results have implications and should set off the studies of other similar gas molecules as well. The controllable diffusion rates by strain can find its applications in filtration, gas separation, and flow control. This approach is simpler than earlier proposed approaches to manipulating the diffusion properties such as changing the elements around the pore edge or synthesizing the PG with larger pores.

4.　Conclusions

In conclusion, the diffusion properties of H_2, O_2 and CO_2 through the unstrained as well as strained porous graphene (PG) were studied by first-principles calculations. The PG can withstand the uniaxial strain up to about 14% and 19% along the armchair and zigzag direction, respectively. The application of strain greatly affects the diffusion barriers, hence the diffusion rate, of the gas molecules. The diffusion rates of H_2, O_2 and CO_2 in PG can be increased up to 2, 5, and 9 orders of magnitude, respectively, using the uniaxial tensile strains of 10% and up to 7, 13, and 20 orders of magnitude, respectively, using the symmetrical stretch strains of 10%. The reasons why the effects of the strains on the diffusion properties are different for different molecules were investigated and explained. Our study suggested that strain manipulation is a valid approach to effectively control the diffusion properties of small molecules such as H_2, O_2 and CO_2 through PG. Because of the significant improvement in the diffusion rates of PG under strain, it is now possible to use strained PG to allow larger molecules such as O_2 through instead of just H_2; opening up wider gas filtering applications of PG.

Acknowledgements

REFERENCES

[1] Tritsaris GA, Vanakaras AG. Two-dimensional ordered porous patterns by molecular design. Langmuir 2010;26(11):7808–12.

[2] Barth JV. Molecular architectonic on metal surfaces. Ann Rev Phys Chem 2007;58(1):375–407.

[3] Bieri M, Treier M, Cai J, Ait-Mansour K, Ruffieux P, Groning O, et al. Porous graphenes: two-dimensional polymer synthesis with atomic precision. Chem Commun 2009;45:6919–21.

[4] Madueno R, Raisanen MT, Silien C, Buck M. Functionalizing hydrogen-bonded surface networks with self-assembled monolayers. Nature 2008;454(7204):618–21.

[5] Schlickum U, Decker R, Klappenberger F, Zoppellaro G, Klyatskaya S, Ruben M, et al. Metal-organic honeycomb nanomeshes with tunable cavity size. Nano Lett 2007;7(12):3813–7.

[6] Ciesielski A, Palma CA, Bonini M, Samorì P. Towards supramolecular engineering of functional nanomaterials: pre-programming multi-component 2D self-assembly at solid-liquid interfaces. Adv Mater 2010;22(32):3506–20.

[7] Koenig SP, Wang L, Pellegrino J, Bunch JS. Selective molecular sieving through porous graphene. Nat Nano 2012;7(11):728–32.

[8] Liu L, Ryu S, Tomasik MR, Stolyarova E, Jung N, Hybertsen MS, et al. Graphene oxidation: thickness-dependent etching and strong chemical doping. Nano Lett 2008;8(7):1965–70.

[9] Fischbein MD, Drndic M. Electron beam nanosculpting of suspended graphene sheets. Appl Phys Lett 2008;93(11). 113107-1–3.

[10] Teweldebrhan D, Balandin AA. Modification of graphene properties due to electron-beam irradiation. Appl Phys Lett 2009;94(1):013101–13103.

[11] Castro Neto AH, Guinea F, Peres NMR, Novoselov KS, Geim AK. The electronic properties of graphene. Rev Mod Phys 2009;81(1):109.

[12] Novoselov KS, Geim AK, Morozov SV, Jiang D, Zhang Y, Dubonos SV, et al. Electric field effect in atomically thin carbon films. Science 2004;306(5696):666–9.

[13] Novoselov KS, Geim AK, Morozov SV, Jiang D, Katsnelson MI, Grigorieva IV, et al. Two-dimensional gas of massless Dirac fermions in graphene. Nature 2005;438(7065):197–200.

[14] Pisula W, Kastler M, Yang C, Enkelmann V, Müllen K. Columnar mesophase formation of cyclohexa-m-phenylene-based macrocycles. Chem Asian J 2007;2(1):51–6.

[15] Li Y, Zhou Z, Shen P, Chen Z. Two-dimensional polyphenylene: experimentally available porous graphene as a hydrogen purification membrane. Chem Commun 2010;46(21):3672–4.

[16] Blankenburg S, Bieri M, Fasel R, Müllen K, Pignedoli CA, Passerone D. Porous graphene as an atmospheric nanofilter. Small 2010;6(20):2266–71.

[17] Ockwig NW, Nenoff TM. Membranes for hydrogen separation. Chem Rev 2007;107(10):4078–110.

[18] Reunchan P, Jhi S-H. Metal-dispersed porous graphene for hydrogen storage. Appl Phys Lett 2011;98(9). 093103-1–3.

[19] Jiang D-E, Cooper VR, Dai S. Porous graphene as the ultimate membrane for gas separation. Nano Lett 2009;9(12):4019–24.

[20] Sint K, Wang B, Král P. Selective ion passage through functionalized graphene nanopores. J Am Chem Soc 2008;130(49):16448–9.

[21] Kohn W, Sham LJ. Self-consistent equations including exchange and correlation effects. Phys Rev 1965;140(4A):A1133.

[22] Kresse G, Furthmüller J. Efficiency of ab-initio total energy calculations for metals and semiconductors using a plane-wave basis set. Comput Mater Sci 1996;6(1):15–50.

[23] Kresse G, Furthmüller J. Efficient iterative schemes for ab initio total-energy calculations using a plane-wave basis set. Phys Rev B 1996;54(16):11169.

[24] Kresse G, Hafner J. Norm-conserving and ultrasoft pseudopotentials for first-row and transition elements. J Phys: Condens Matter 1994;6(40):8245.

[25] Perdew JP, Burke K, Ernzerhof M. Generalized gradient approximation made simple. Phys Rev Lett 1996;77(18):3865.

[26] Ceperley DM, Alder BJ. Ground state of the electron gas by a stochastic method. Phys Rev Lett 1980;45(7):566.

[27] Blöchl PE. Projector augmented-wave method. Phys Rev B 1994;50(24):17953.

[28] Kresse G, Joubert D. From ultrasoft pseudopotentials to the projector augmented-wave method. Phys Rev B 1999;59(3):1758.

[29] Du A, Zhu Z, Smith SC. Multifunctional porous graphene for nanoelectronics and hydrogen storage: new properties revealed by first principle calculations. J Am Chem Soc 2010;132(9):2876–7.

[30] Becke AD, Edgecombe KE. A simple measure of electron localization in atomic and molecular systems. J Chem Phys 1990;92(9):5397–403.

[31] Silvi B, Savin A. Classification of chemical bonds based on topological analysis of electron localization functions. Nature 1994;371(6499):683–6.

[32] Renka RJ. Algorithm 752: SRFPACK: software for scattered data fitting with a constrained surface under tension. ACM Trans Math Softw 1996;22(1):9–17.

[33] Greaves GN, Greer AL, Lakes RS, Rouxel T. Poisson's ratio and modern materials. Nat Mater 2011;10(11):823–37.

[34] Şahin H, Cahangirov S, Topsakal M, Bekaroglu E, Akturk E, Senger RT, et al. Monolayer honeycomb structures of group-IV elements and III-V binary compounds: first-principles calculations. Phys Rev B 2009;80(15):155453.

[35] Lee C, Wei X, Kysar JW, Hone J. Measurement of the elastic properties and intrinsic strength of monolayer graphene. Science 2008;321(5887):385–8.

[36] Topsakal M, Cahangirov S, Ciraci S. The response of mechanical and electronic properties of graphane to the elastic strain. Appl Phys Lett 2010;96(9):091912–91913.